JACS
JOURNAL OF THE AMERICAN CHEMICAL SOCIETY
pubs.acs.org/JACS
Article

Exponential Amplification Using Photoredox Autocatalysis

Seunghyeon Kim, Alejandra Martínez Dibildox, Alan Aguirre-Soto, and Hadley D. Sikes*

Cite This: J. Am. Chem. Soc. 2021, 143, 11544–11553
Read Online
ACCESS | Metrics & More | Article Recommendations | Supporting Information

ABSTRACT: Exponential molecular amplification such as the polymerase chain reaction is a powerful tool that allows ultrasensitive biodetection. Here, we report a new exponential amplification strategy based on photoredox autocatalysis, where eosin Y, a photocatalyst, amplifies itself by activating a nonfluorescent eosin Y derivative (EYH^{3-}) under green light. The deactivated photocatalyst is stable and rapidly activated under low-intensity light, making the eosin Y amplification suitable for resource-limited settings. Through steady-state kinetic studies and reaction modeling, we found that EYH^{3-} is either oxidized to eosin Y via one-electron oxidation by triplet eosin Y and subsequent $1e^-/H^+$ transfer, or activated by singlet oxygen with the risk of degradation. By reducing the rate of the EYH^{3-} degradation, we successfully improved EYH^{3-}-to-eosin Y recovery, achieving efficient autocatalytic eosin Y amplification. Additionally, to demonstrate its flexibility in output signals, we coupled the eosin Y amplification with photoinduced chromogenic polymerization, enabling sensitive visual detection of analytes. Finally, we applied the exponential amplification methods in developing bioassays for detection of biomarkers including SARS-CoV-2 nucleocapsid protein, an antigen used in the diagnosis of COVID-19.

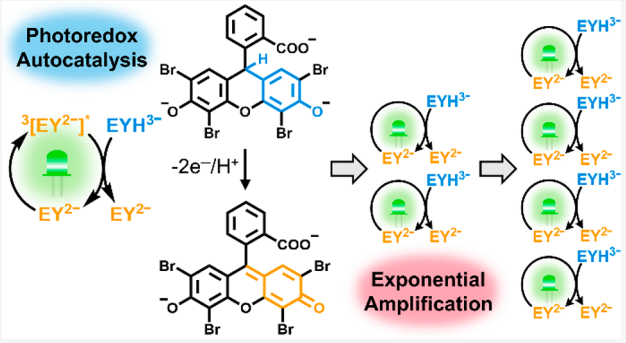

INTRODUCTION

The development of rapid, affordable, and highly sensitive biodetection methods for resource-limited settings is of paramount importance in the detection and diagnosis of infectious diseases. Advances in point-of-care diagnostic tests have enabled rapid detection of high concentrations of biomarkers at low cost,[1,2] but these tests have limited utility for clinical decision-making due to lower sensitivity[3−5] than other laboratory methods such as the polymerase chain reaction (PCR). PCR can detect low-abundance target nucleic acids[6] or antigens (via immuno-PCR)[7] by amplifying specific nucleic acids exponentially, but this method often takes several hours and is not easily translated to resource-limited settings due to reliance on laboratory instruments (thermal cyclers and analyzers), poor stability of enzyme-based reagents, and requirement of trained personnel.[8−10] To address these issues, efforts have been made to develop isothermal nucleic acid amplification strategies,[9,11] long-term storage methods for reagents,[12] and automated formats.[9,11,13]

Alternatively, several research groups are dedicated to the development of non-PCR exponential molecular amplification methods by the careful design of small molecule amplification reagents. These reagents can amplify activating molecules such as acetate,[14] hydrogen peroxide,[15−17] fluoride,[18−22] thiol,[23] piperidine,[24] and photosensitizers[25,26] through autoinductive or autocatalytic reactions[27,28] such as activation of a supramolecular catalyst,[14] a cascade of self-immolative reactions,[15−24] and photounmasking of photosensitizers.[25,26] However, despite the successful detection of analytes in aqueous solutions such as enzymes,[15] nerve agents,[22,23] metal ions,[19,24] and avidin,[26] these amplification methods have never been used to detect biomarkers of infectious diseases.

To address this gap, broadly applicable exponential amplification methods for sensitive biodetection need to be developed with the following considerations. First, the activating molecules should be easily conjugated to affinity reagents or liberated from the conjugated probes, amplifying signals associated with specific binding events. Second, the amplification reagents should be thermally stable for long-term storage without refrigeration, and soluble in water to avoid the handling of flammable and toxic organic solvents by untrained users. Furthermore, the amplification time should be short (within minutes) and readily controlled with external stimuli such as heat and light to prevent false positive results and provide quantitative information. Most importantly, autoinductive cascade or autocatalysis should be carefully designed to achieve exponential amplification of biodetection signals.

Herein, we demonstrate a new exponential signal amplification strategy based on photoredox autocatalysis,

Received: April 22, 2021
Published: July 21, 2021

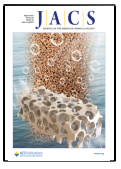

https://doi.org/10.1021/jacs.1c04236
J. Am. Chem. Soc. 2021, 143, 11544−11553

which can be applied to various biodetection assays. Inspired by the activation of nonfluorescent probes such as **1** and **2** via photoinduced oxidation (Scheme 1A),[29−34] we designed eosin

Scheme 1. (A) General Activation Pathway of Dihydroxanthene Dyes (1 and 2). (B) Hypothesized Activation Pathway of EYH^{3-} to EY^{2-} via Photoredox Autocatalysis (Present Work)[a]

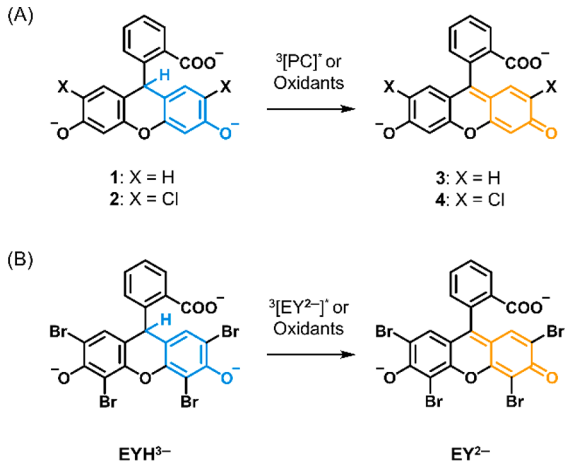

[a]^3[PC]*: photocatalyst in triplet excited state. ^{3}[EY^{2-}]*: triplet EY^{2-}.

Y (EY^{2-})-based photoredox autocatalysis where doubly reduced and protonated eosin Y (EYH^{3-}) is converted into EY^{2-} by triplet EY (^{3}[EY^{2-}]*) or other oxidizing species produced during the photoredox catalysis of EY^{2-} (Scheme 1B). EY^{2-} was chosen as the photocatalyst for the autocatalytic reaction because (1) EY^{2-}-conjugated affinity reagents can be readily prepared,[35−37] (2) EY^{2-} has a high triplet quantum yield (0.6−0.7)[38,39] and a long triplet lifetime (1.85 ms)[40] in water, (3) EYH^{3-} cannot absorb visible light,[41,42] (4) both EY^{2-} and EYH^{3-} are water-soluble due to ionizable groups, and (5) EYH^{3-} is potentially stable against oxidation during storage.[41,43]

Our initial hypothesis was that the additional EY^{2-} generated in previous photoredox cycles can activate EYH^{3-} in the next cycle, so it was expected that the amount of EY^{2-} would increase exponentially (Scheme 2). However, the quenching of activating molecules and other side reactions could hamper efficient activation of EYH^{3-} and cause degradation of EY^{2-} and EYH^{3-}. To enhance the kinetics and efficiency of the autocatalytic reaction, we studied the mechanism of EY amplification. Employing the mechanistic insights from the steady-state kinetic studies and reaction modeling, we could dramatically improve EYH^{3-}-to-EY^{2-} recovery and achieve a rapid and sensitive autocatalytic EY amplification.

Additionally, we demonstrate that the autocatalytic EY amplification can be coupled with other photochemical reactions to generate different forms of signals. After combining the EY amplification with oxidative polymerization of 3,3′-diaminobenzidine (DAB), the amplification system produced colorimetric signals with brown insoluble polymer. Finally, we applied the exponential amplification methods in developing bioassays for detection of biomarkers including SARS-CoV-2 nucleocapsid protein, an antigen used to diagnose COVID-19.

Scheme 2. Autocatalytic Amplification of EY^{2-}[a]

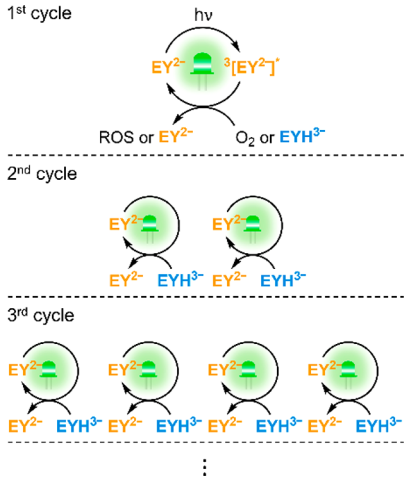

[a]Triplet EY^{2-} (^{3}[EY^{2-}]*) is either quenched by oxygen (O_2) to generate reactive oxygen species (ROS) or oxidizes EYH^{3-} to produce EY^{2-}. The amplification reagent (EYH^{3-}) is activated by a small amount of EY^{2-} in an autocatalytic manner to amplify the number of EY^{2-} in the system.

RESULTS AND DISCUSSION

Synthesis and Characterization of EYH^{3-}. Synthesis of EYH^{3-} was achieved by reducing 1,4-benzoquinone-like structure of EY^{2-} to hydroquinone-like structure with sodium borohydride in aqueous solution as described in Figure 1A,[42]

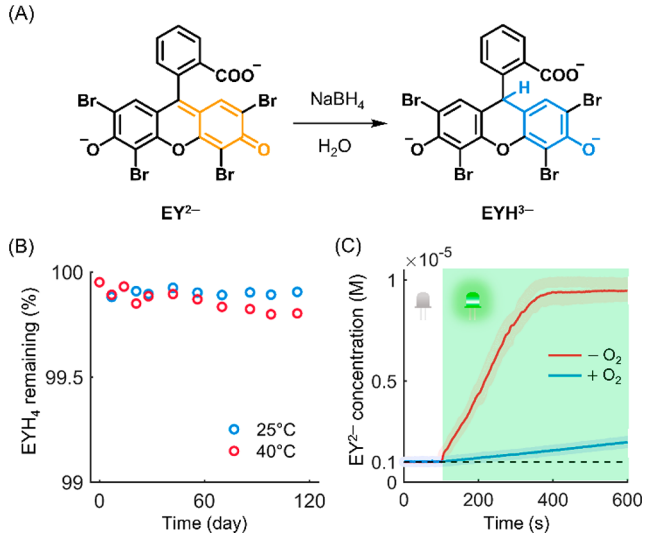

Figure 1. Synthesis and characterization of the amplification reagent (EYH^{3-}). (A) Synthesis of EYH^{3-}. (B) Thermal stability of protonated EYH^{3-} (EYH_4) in DMSO at 25 and 40 °C. (C) Activation of 8.6 μM EYH^{3-} by 1 μM EY^{2-} in 0.2 M phosphate buffer (pH 7.4) under 2.6 mW/cm^2 green light (λ_{max} = 535 nm) in deaerated and air-saturated solutions.

leading to a loss of conjugation in the π-system. It should be noted that EY^{2-} and EYH^{3-} represent fully deprotonated forms of eosin Y and dihydroeosin Y in this paper. Because of the ionizable groups in EYH^{3-}, it is soluble in neutral-to-high pH solutions, but its solubility decreases as pH decreases. Thus, EYH^{3-} was easily purified by precipitation to EYH_4 at low pH

https://doi.org/10.1021/jacs.1c04236
J. Am. Chem. Soc. 2021, 143, 11544−11553

and then stored in DMSO (see the Materials and Methods in Supporting Information).

By monitoring EY^{2-} and EYH^{3-} concentrations in the EYH^{3-} solution, we confirmed the long-term (at least 4 months) stability of EYH_4 at 25 °C (Figure 1B). With the consideration that the EYH_4 stock solutions in DMSO were kept in centrifuge tubes without airtight sealing, the results support the high stability of protonated EYH_4 against oxidation in DMSO at 25 °C although the oxidation is slightly faster at 40 °C.

Next, we tested if EYH^{3-} could be photoactivated by EY^{2-} in deaerated and air-saturated solutions (Figure 1C). In both conditions, EYH^{3-} was activated to generate EY^{2-} upon light irradiation, but the EY amplification rates were very different. Interestingly, in the deaerated solution, EY^{2-} generation was much faster without the potential terminal oxidant (oxygen) than in the air-saturated solution, and the EY^{2-} concentration reached 9.6 μM, implying 100% EYH^{3-}-to-EY^{2-} recovery. The EY^{2-} concentration in air-saturated solution did not reach 4 μM even after extended illumination (30 min). Unfortunately, oxygen must be included in the EY amplification system because removing oxygen in practical settings is not feasible, and the amplification should occur as fast as possible. Thus, we sought to improve our mechanistic understanding of the oxygen-free EY amplification and the role of oxygen to achieve a more rapid and sensitive autocatalytic amplification method by removing inefficiencies in the system.

Investigation of EY Amplification Mechanism. Using UV−vis spectroscopy, we monitored the steady-state kinetics of EY amplification in deaerated and air-saturated solutions (pH 7.4) (Figures 2A and S7). On the basis of kinetic analysis, we proposed elementary reactions associated with EYH^{3-} activation and integrated them into the reported photochemical reactions of EY^{2-} (Table S1). To estimate unknown parameters and validate the proposed reactions, we first developed the simplest kinetic model for one-species system (EY^{2-}), where all rate constants could be obtained from literature, and increased complexity of the model by adding other species (EYH^{3-} and O_2) and associated reactions to the system (see the Model Development section in Supporting Information for details on reaction mechanism and kinetic modeling).

When the deaerated solutions including EY^{2-} and EYH^{3-} are irradiated with green light, EY^{2-} is excited to singlet state ($^1[EY^{2-}]^*$) (Table S1, eq 1), whose energy is lost through vibrational relaxation and internal conversion (eq 2), fluorescence (eq 3), and intersystem crossing (eq 4). The triplet EY^{2-} ($^3[EY^{2-}]^*$) generated from intersystem crossing either decays via phosphorescence (eq 5) and energy transfer to EY^{2-} (eq 6) and EYH^{3-} (eq 8), or activates EYH^{3-} via reductive quenching (eq 7), which produces $EY^{\bullet 3-}$ and one-electron oxidized EYH^{3-}. At neutral pH, the singly oxidized EYH^{3-} appears to lose $1e^-/1H^+$ through intermolecular reactions with the singly oxidized EYH^{3-}, EYH^{3-}, and other buffer components to become EY^{2-}, producing H_2 or other side products (Figure S8). The hydrogen evolution[44,45] may drive the EY amplification even without oxygen as a terminal oxidant. Lastly, the fate of $EY^{\bullet 3-}$ radicals can be described with acid−base equilibria (eqs 9−10) in phosphate buffer solutions (pH 7.4) and pH-dependent disproportionation reactions (eqs 11−13).[31]

The kinetic model constructed with this mechanism provided consistent results with the concentration profiles of

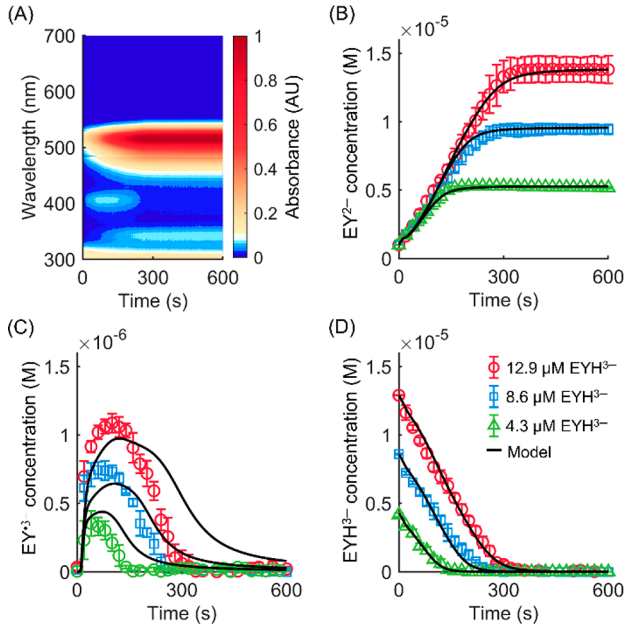

Figure 2. Steady-state kinetic studies of EY amplification in deaerated solutions. Various concentrations (4.3, 8.6, and 12.9 μM) of EYH^{3-} with 1 μM EY^{2-} in deaerated solutions were irradiated under 2.6 mW/cm^2 green light (λ_{max} = 535 nm). In these conditions, the EY^{2-} impurity from the EYH^{3-} stock solution accounted for only 0.65% of total initial EY^{2-} at most, which was within experimental errors. (A) Heatmap plot of UV−vis absorbance change over time. Colormap was adjusted to clearly show formation of transient species, $EY^{\bullet 3-}$, at 405 nm. Absorbance vs wavelength graph is also available in Figure S7. Steady-state kinetics of (B) EY^{2-} monitored at 516 nm, (C) $EY^{\bullet 3-}$ monitored at 405 nm, and (D) EYH^{3-} monitored at 312 nm during the irradiation. Black solid lines demonstrate the concentration of each species predicted by a kinetic model.

EY^{2-} and EYH^{3-} (Figure 2B,D). However, the concentration profile of $EY^{\bullet 3-}$ was not perfectly predicted by the model. One reason for the discrepancy is that the radical concentration is particularly sensitive to kinetic parameters obtained from literature, which were measured or estimated in slightly different conditions. Another possibility is that the model ignored the oxygen dissolution and diffusion from a potential leak of air. Indeed, the concentration of $EY^{\bullet 3-}$ could be very sensitive to the leak because the oxidation of $EY^{\bullet 3-}$ by oxygen is almost a diffusion-controlled reaction (1×10^9 M^{-1} s^{-1}).[46] By considering the exposure to oxygen, the model could better predict the radical concentration profile (Figure S12). However, we confirmed that even if we carefully prevented the leak, we still observed faster decay of $EY^{\bullet 3-}$ than the model prediction (Figure S13). Therefore, we concluded that there might be other unidentified radical decay processes under light because we have already counted the radical decay rates in the dark. The unexpectedly fast radical decay was also observed in fluorescein[31] and erythrosine[47] particularly at high pH, implying that the dye triplets may react with hydroxide ions to form oxidizing radicals. Although the additional radical decay processes would not significantly alter the EY amplification kinetics in air-saturated solutions, we expect that if reaction mechanisms for these processes were elucidated and considered in the model, the concentration of $EY^{\bullet 3-}$ would be better predicted by the model (Figure 2C).

Notably, in deaerated conditions, two EYH^{3-} activation reactions (two EY radicals) are required to produce one

https://doi.org/10.1021/jacs.1c04236
J. Am. Chem. Soc. 2021, 143, 11544−11553

additional EY^{2-} molecule due to the nature of disproportionation reactions (eqs 11,12). In air-saturated solutions, one EYH^{3-} activation leads to one EY^{2-} production because $EY^{\bullet 3-}$ is rapidly oxidized to EY^{2-} by oxygen (~0.25 mM),[48] producing superoxide ($O_2^{\bullet -}$) (eq 14) and hydrogen peroxide (H_2O_2) through a series of reactions (eqs 15−20).[49] However, as shown in Figure 1C, the EY amplification becomes sluggish in the presence of oxygen, which is mainly because of the physical quenching of $^3[EY^{2-}]^*$ by oxygen, producing ground-state EY^{2-} and $^1O_2$ (eq 21).[46,50] The singlet oxygen is known to decay through interactions with solvent (eq 22)[51] and dissolved oxygen (eq 23).[30]

The kinetic model updated with the above reactions could not predict the trend of experimental data (Figure S15). The model provided much slower EYH^{3-} activation than experimental data and 100% recovery of EYH^{3-} to EY^{2-}, but in reality, significant loss of EY species (EY^{2-}, $EY^{\bullet 3-}$, and EYH^{3-}) occurred during EY amplification in the presence of oxygen. To address this deviation, we focused on the reactivity of $^1O_2$, which is one of the most reactive species that is generated in the system and has higher energy by 94 kJ/mol than the ground-state oxygen.[52] The singlet oxygen has been proposed as the oxidant for other dihydroxanthene dyes previously[30,34] and is known to oxidize hydroquinone to benzoquinone,[53] so $^1O_2$ is plausible to contribute to EYH^{3-} oxidation (eq 24). Additionally, $^1O_2$ has been reported to participate in Diels−Alder type reactions on various chromophores such as anthracenes and perylenes, which results in a loss of conjugation.[54−57] Substituted phenols can rapidly react with $^1O_2$ to yield oxygenated products.[58,59] Therefore, the oxidation of EYH^{3-} and EY^{2-} by $^1O_2$ could be disruptive, which leads to degradation of EYH^{3-} (eq 25) and EY^{2-} (eq 26). These $^1O_2$-driven reactions (eqs 24−26) were experimentally confirmed using a $^1O_2$ quencher (sodium azide) and a $^1O_2$ enhancer (deuterium oxide) (Figure S16). Updated with these $^1O_2$-driven activation and degradation reactions, the model successfully described the EY amplification kinetics and EYH^{3-}-to-EY^{2-} recovery (model: 34.3%; experiment: 34.5%) in air-saturated solutions (Figure 3A).

Optimization of EY Amplification with Insights from the Mechanism. From the proposed mechanism for EY amplification (Scheme 3), where EYH^{3-} is oxidized to EY^{2-} by $^3[EY^{2-}]^*$ and $^1O_2$, we identified reactions retarding the EY amplification in air-saturated solution: (1) quenching of $^3[EY^{2-}]^*$ by oxygen and (2) degradation of EYH^{3-} by $^1O_2$. Although the triplet quenching was facilitated by high concentration of oxygen (~0.25 mM) compared to that of EYH^{3-} (~12 μM), increasing light intensity could raise the $^3[EY^{2-}]^*$ production rate, enhancing kinetics of EYH^{3-} oxidation by the triplet. However, according to the model, this measure might not improve the recovery of EYH^{3-} to EY^{2-} because faster degradation of EYH^{3-} and EY^{2-} by $^1O_2$ could be accompanied by the increased light intensity, limiting the maximum concentration of amplified EY^{2-} (Figure S18). Thus, to improve the amplification factor ($[EY^{2-}]_{final}/[EY^{2-}]_{initial}$), it is of primary importance to increase the recovery by preventing the $^1O_2$-involved degradation of EYH^{3-} and EY^{2-}.

Considering that the yield of photosensitized $^1O_2$ production can be dependent on pH because the degree of protonation in triplet photosensitizers may impact the energy transfer to ground-state oxygen,[60,61] we investigated the effects

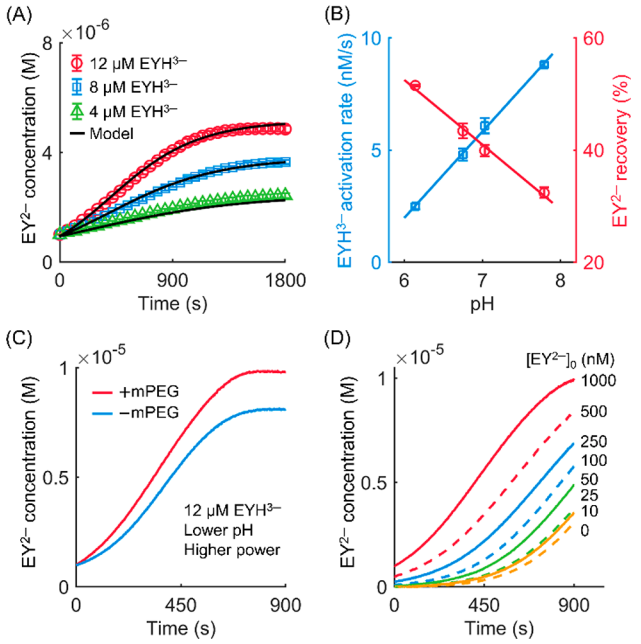

Figure 3. Steady-state kinetic studies of EY amplification in the presence of oxygen. Various concentrations (4, 8, and 12 μM) of EYH^{3-} with 1 μM EY^{2-} and ~0.25 mM oxygen[48] were irradiated under 1.2 mW/cm^2 green light (λ_{max} = 535 nm). (A) Steady-state kinetics of EY amplification monitored at 516 nm during the irradiation. Black solid lines show EY^{2-} concentration predicted by a kinetic model. (B) pH dependence of EYH^{3-} activation rate and EY^{2-} recovery from EYH^{3-}. (C) Impact of methoxy poly(ethylene glycol) (mPEG, 20 mM) on the EY^{2-} recovery. Lower pH, 6, and higher power, 3.6 mW/cm^2(λ_{max} = 530 nm), were used to improve the EY^{2-} recovery and the EYH^{3-} activation rate. The graph shows sigmoidal increase in EY^{2-} concentration. (D) EY^{2-} is amplified as EYH^{3-} is consumed, enabling to detect EY^{2-} as low as 10 nM using a UV−vis spectrometer with a detection limit of 50 nM EY^{2-}. The amplification reagent was composed of 12 μM EYH^{3-} and 40 mM mPEG in 0.2 M phosphate buffer (pH 6).

of pH on EY amplification. As shown in Figure 3B, the recovery increased from 34% to 52% as pH decreased from 7.8 to 6.1 whereas the EYH^{3-} oxidation rate decreased likely because of pH-dependent photoactivity of eosin Y.[62] At present, it is not clear whether $^1O_2$ quantum yield was reduced or the rate of EYH^{3-} degradation by $^1O_2$ decreased at low pH by protonation (pK_a = 6.5, Figure S9) of EYH^{3-}, but lowering pH was very effective to improve the recovery. Therefore, we used pH 6 phosphate buffer (0.2 M) for the following experiments and increased light intensity to compensate for the reduction in EYH^{3-} oxidation rate. In addition, we confirmed that residual DMSO from the EYH^{3-} stock solution did not affect the EY amplification kinetics (Figure S19), supporting DMSO as a safe storage solvent for EYH_4.

As another approach to suppressing the EYH^{3-} and EY^{2-} degradation by $^1O_2$, we included methoxy poly(ethylene glycol) (mPEG) in the buffer solution because localization of EY^{2-} and EYH^{3-} in carbon-rich mPEG phase could increase the rate of EYH^{3-} oxidation by $^3[EY^{2-}]^*$ relatively to reaction rates between $^1O_2$ and EYH^{3-} and might also cause faster depletion and slower replenishment of oxygen,[63] inhibiting $^1O_2$ production. Surprisingly, the recovery increased to 74% when the buffer solution including mPEG was irradiated under higher light intensity (3.6 mW/cm^2) (Figure 3C). Even higher recovery (91%) could be obtained with 10 mW/cm^2 green

https://doi.org/10.1021/jacs.1c04236
J. Am. Chem. Soc. 2021, 143, 11544−11553

Scheme 3. Mechanism of EY Autocatalytic Amplification through Photosensitized Oxidation of EYH^{3-}[a]

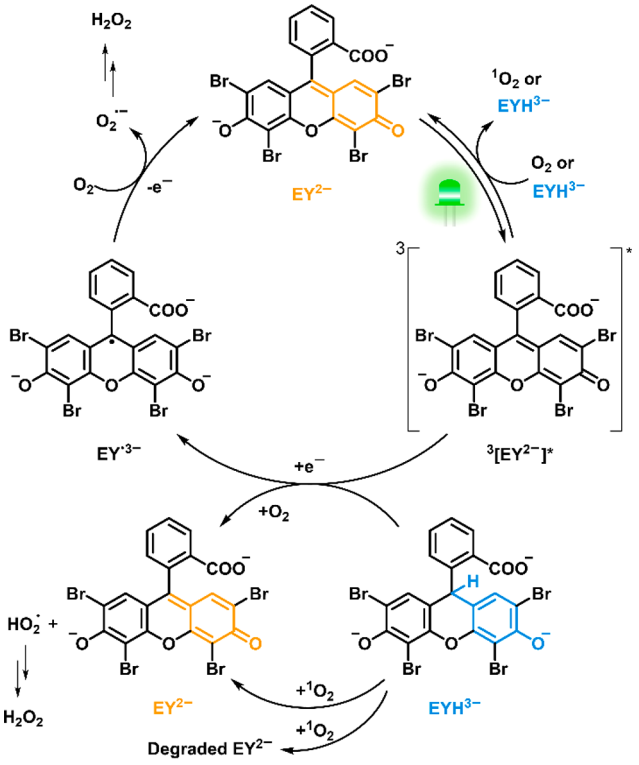

[a] EY^{2-} is photoreduced by EYH^{3-} upon absorption of green light. $EY^{\bullet 3-}$ is rapidly oxidized back to EY^{2-} via single electron transfer to oxygen. The oxidized EYH^{3-} reacts with oxygen to yield EY^{2-} and hydroperoxyl radical. Singlet oxygen, generated by energy transfer from $^3[EY^{2-}]^*$ to ground-state oxygen, not only activates EYH^{3-} but also degrades the inactivated eosin Y.

light (Figure S20) likely due to faster oxygen depletion in the mPEG phase. Together with enhanced light intensity, it also clearly displayed a sigmoidal response curve, which is a typical indicator of autocatalytic reactions.[27,28] We excluded $^1O_2$ quenching by mPEG because the lifetime of $^1O_2$ does not change in PEG solution.[64] Excited states kinetics (e.g., triplet lifetime) of EY^{2-} could change with the mPEG addition as reported in other environments,[65] but longer triplet lifetime (simulated by ignoring all decay pathways except for quenching by oxygen) could provide only minor improvement (~1%) in the recovery. Thus, it is reasonable to propose that the nanoscale liquid−liquid phase separation locally concentrates EY^{2-} and EYH^{3-} and selectively increases the rate of oxygen-free EYH^{3-} oxidation, assisting to improve the recovery.

After optimizing the mPEG concentration (Figure S21), we performed EY amplification experiments with various initial concentrations of EY^{2-} (Figure 3D). Under 3.6 mW/cm^2 green light, EY^{2-} was successfully amplified with 12 μM EYH^{3-} and 40 mM mPEG in 0.2 M phosphate buffer (pH 6), the amplification factor ($[EY^{2-}]_{final}/[EY^{2-}]_{initial}$) after 900 s of irradiation could increase up to 500 (Figure S22), and the limit of detection for this proof-of-concept EY^{2-} detection assay was 10 nM. With the consideration that the UV−vis spectrophotometer used in the experiments could not detect below 50 nM EY before the amplification, this is an exciting demonstration that the autocatalytic EY amplification strategy is capable of improving the assay sensitivity.

Coupling EY Amplification with DAB Polymerization. Importantly, the EY amplification can be coupled with various photochemical reactions to generate different forms of signals. To demonstrate this potential, we combined the EY amplification with photoinduced oxidative polymerization of 3,3′- diaminobenzidine (DAB). Because DAB is known to form a brown-colored phenazine polymer when oxidized by $^1O_2$ or $O_2^{\bullet -}$,[35,66,67] we expected that the incorporation of DAB would also contribute to improving the EYH^{3-}-to-EY^{2-} recovery by consuming $^1O_2$ in addition to producing colorimetric signals, which has proven to be true (Figure S23). Interestingly, there was an unexpected synergy in the EY-DAB amplification. As proposed in Figure 4A, EYH^{3-} can be

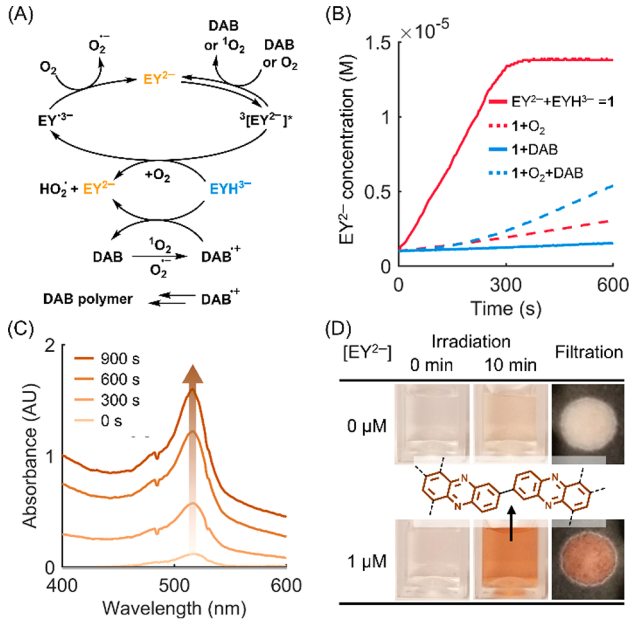

Figure 4. EY amplification coupled with 3,3′-diaminobenzidine (DAB) polymerization. (A) Mechanism of the EY-DAB amplification. EYH^{3-} is activated not only by $^3[EY^{2-}]^*$, but also by oxidized DAB radicals ($DAB^{\bullet +}$) formed from DAB and $^1O_2$ or $O_2^{\bullet -}$ reaction. The $DAB^{\bullet +}$ also reacts with each other to form brown polymer. Detailed reaction mechanism for EY and DAB is available in ref.[66] (B) Steady-state kinetic studies of EY amplification with oxygen and DAB. System **1** included only 1 μM EY^{2-} and ~12 μM EYH^{3-} in pH 7.4 phosphate buffer (0.2 M). The concentrations of added oxygen and DAB were ~0.25 mM and 0.6 mM, respectively. (C) Absorbance change during EY-DAB amplification under 3.6 mW/cm^2 green light (λ_{max} = 530 nm). The solution included 1 μM EY^{2-}, 12 μM EYH^{3-}, and 0.6 mM DAB in 0.2 M Na_2HPO_4(pH 9). (D) Visual detection of 1 μM EY^{2-} using EY-DAB amplification. The same conditions as described in (C) apply here. After 10 min EY-DAB amplification, brown phenazine polymer formed in the solution with 1 μM EY^{2-}, which can be filtered by cellulose paper.

activated by the oxidized DAB radicals ($DAB^{\bullet +}$) formed from the reaction between DAB and $^1O_2$ or $O_2^{\bullet -}$, meaning that the side products of EY amplification can be recycled by DAB to activate more EYH^{3-}. This is supported by kinetic studies of EY amplification with oxygen and DAB (Figure 4B). Compared to system **1** including only EY^{2-} and EYH^{3-}, addition of either oxygen or DAB to **1** retarded EY amplification due to rapid quenching of $^3[EY^{2-}]^*$ by the

https://doi.org/10.1021/jacs.1c04236
J. Am. Chem. Soc. 2021, 143, 11544−11553

additives. When both oxygen and DAB were added to **1**, the EY amplification rate did not further decrease, but increased. Together with the higher recovery with DAB, this counterintuitive result indicates that $DAB^{\bullet+}$ can activate EYH^{3-} less disruptively than $^1O_2$.

After optimizing conditions for EY-DAB amplification to maximize EY-specific polymerization response (Figures S24–S26), we proceeded to the visual detection of EY^{2-} in solution. As shown in Figure 4C, EY-DAB amplification increases not only the absorbance (λ_{max} = 516 nm) of EY^{2-} but also the absorbance in the visible range (400–700 nm) in the presence of EY^{2-} (1 μM). This broad absorption band is attributed to the insoluble DAB polymer, which enables visual detection of 1 μM EY^{2-} in solution (Figure 4D).

Application of EY Amplification in Biodetection Assays. Finally, we applied the EY and EY-DAB amplification strategies to specific detection of biomolecules. First, we developed a rapid (<30 min) cellulose particle-based fluorescence assays with EY amplification to detect SARS-CoV-2 nucleocapsid protein (N-protein), a biomarker of COVID-19.[68−70] As described in Figure 5A, capture binder

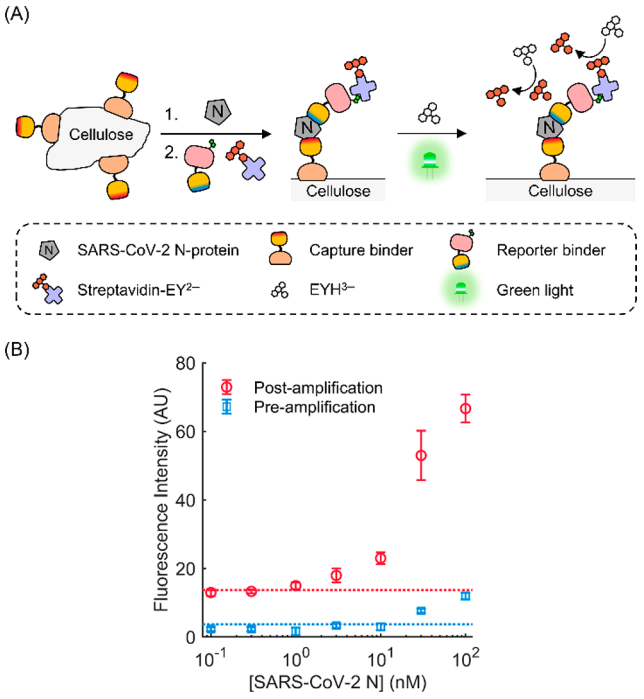

Figure 5. Detection of SARS-CoV-2 N-protein using cellulose-based fluorescence assay with EY amplification. (A) Schematic description of the assay. Detailed protocol and conditions are available in the Supporting Methods section. (B) SARS-CoV-2 N-protein fluorescence assay results before and after EY amplification. The EY amplification improved the detection limit of SARS-CoV-2 N-protein by ~30-fold from 30 nM (preamplification, blue square) to 1 nM (postamplification, red circle). The dotted line (Neg+3σ) represents the mean fluorescence intensity (Neg) of 0 nM samples plus three times their standard deviation (σ) for each case.

(SsoNP.E2)[71] is genetically fused to cellulose binding domain (CBD) for oriented immobilization on microcrystalline cellulose particles. Once SARS-CoV-2 N-protein (0–100 nM) in samples is captured on the cellulose particles, the captured target is labeled with reporter binder (SsoNP.E1 fused to biotinylated maltose binding domain)[71] and EY^{2-}-conjugated streptavidin (streptavidin-EY). The fluorescence intensity from EY^{2-} associated with the captured target is then amplified by oxidizing EYH^{3-} for 10 min under green light (5 mW/cm^2, λ_{max} = 530 nm). As can be seen in Figure 5B, the EY amplification improved the detection limit of the N-protein by ~30-fold from 30 nM to 1 nM, which is in the range for detecting live, replicating viruses.[72−75] Although there are more sensitive assays for SARS-CoV-2 viral RNA detection using reverse transcription loop-mediated isothermal amplification (RT-LAMP)[76,77] or electrochemical biosensor,[78] the N-protein detection approach has greater potential for healthy population screening[79] because it is free of complicated RNA extraction before testing, and the positive N-protein results better indicate potential transmissibility than the RNA detection methods.[80−82]

Next, we incorporated EY-DAB amplification into colorimetric assays. Using the same cellulose particle-based platform, we detect streptavidin-EY^{2-} as a model protein with capture binder (rcSso7d.SA) genetically fused to CBD.[83] As presented in Figure 6A, after the target protein is captured on the

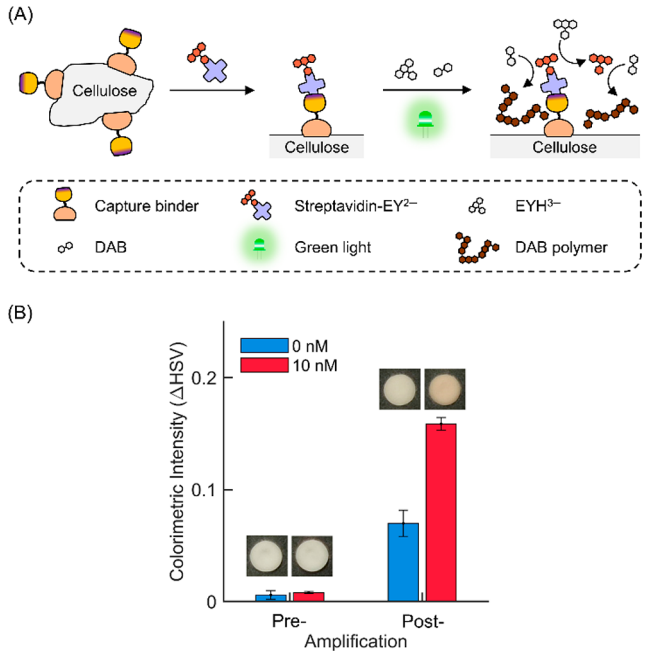

Figure 6. Detection of EY^{2-}-conjugated streptavidin (streptavidin-EY^{2-}) using cellulose-based colorimetric assay with EY-DAB amplification. (A) Schematic description of the assay. Detailed protocol and conditions are available in the Supporting Information. (B) Streptavidin-EY^{2-} colorimetric assay results before and after EY-DAB amplification. Representative images are provided above corresponding bar graphs. Images for replicates are available in Figure S27. Colorimetric intensity was calculated in HSV (Hue, Saturation, Value) color space using a reported method in literature.[84]

cellulose particles, EY-DAB amplification reagents are added and irradiated under green light to produce the brown polymer. Comparing pre- and postamplification results in Figure 6B, we can see that the EY-DAB amplification allows visual detection of 10 nM streptavidin-EY^{2-}.

These proof-of-concept assays reveal that the autocatalytic EY amplification strategy using water-soluble, thermally stable, and rapidly activatable EYH^{3-} can be easily incorporated into various types of biodetection assays using EY-conjugated affinity reagents. Additionally, the method can improve the

https://doi.org/10.1021/jacs.1c04236
J. Am. Chem. Soc. 2021, 143, 11544−11553

detection limit by amplifying biodetection signals with low-intensity light (5 mW/cm^2), so it could be especially useful with low-cost, portable, but not very sensitive fluorescent reader or imaging setup as opposed to sophisticated instruments in centralized laboratories. Because the EY amplification is not significantly influenced by the temperature-dependent oxygen concentration in the amplification reagents (Figure S28), the EY amplification may be used at the point of care without major complications.

In this paper, the assays were tested only with target molecules spiked in buffer solutions (1% Triton X-100 in 1 × PBS) instead of clinical samples such as saliva or nasal swab samples, whose components may contribute to change in the EY amplification kinetics (Figure S29). Therefore, reaction conditions should be optimized depending on the sample matrix. Currently, the EY^{2-} impurity (0.05%, 6 nM) in the amplification reagents including 12 μM EYH^{3-} induces the autocatalytic EY amplification even without target-associated EY^{2-}, increasing background signals and negatively affecting the detection limit. Given that red light-absorbing photosensitizers such as methylene blue (MB) can oxidize other dihydroxanthene dyes,[34,85] strategies to design red-light photocatalytic activation of EYH^{3-} using target-associated MB followed by autocatalytic EY amplification under green light would be a promising future direction to improve the detection limit because no EYH^{3-} will be activated by the EY^{2-} impurity under red light.

CONCLUSION

In summary, we developed an autocatalytic signal amplification method for sensitive biodetection by employing the photocatalytic activation of EYH^{3-}. This inactivated photocatalyst is easily prepared, water-soluble, thermally stable, and rapidly activated by $^3[EY^{2-}]^*$ and $^1O_2$ produced during photocatalysis of EY^{2-}, amplifying the amount of EY^{2-} in aqueous solution. The EY amplification can also be coupled with various photochemical reactions to produce different forms of signals. To demonstrate this potential, DAB polymerization was combined with EY amplification to enable visual detection of EY^{2-}. Furthermore, using EY^{2-}-conjugated affinity reagents, we developed a fluorescence assay for detection of SARS-CoV-2 nucleocapsid protein, a biomarker of COVID-19, and a colorimeric assay for detection of streptavidin, revealing that the EY amplification strategy can be easily adopted to amplify biodetection signals in different kinds of assays. Considering the long shelf life of EYH^{3-} $^{3-}$and the rapid EY amplification under low-intensity light, we anticipate that this nonenzymatic autocatalytic amplification reaction is especially useful in developing rapid and highly sensitive point-of-care assays.

ASSOCIATED CONTENT

Supporting Information

The Supporting Information is available free of charge at https://pubs.acs.org/doi/10.1021/jacs.1c04236.

Materials and methods; model development (PDF)

AUTHOR INFORMATION

Corresponding Author

Hadley D. Sikes − *Department of Chemical Engineering, Massachusetts Institute of Technology, Cambridge, Massachusetts 02139, United States; Antimicrobial Resistance Integrated Research Group, Singapore-MIT Alliance for Research and Technology, Singapore 138602, Singapore;* orcid.org/0000-0002-7096-138X; Email: sikes@mit.edu

Authors

Seunghyeon Kim − *Department of Chemical Engineering, Massachusetts Institute of Technology, Cambridge, Massachusetts 02139, United States;* orcid.org/0000-0001-6515-2679

Alejandra Martínez Dibildox − *School of Engineering and Sciences, Tecnologico de Monterrey, Monterrey, N.L. 64849, Mexico*

Alan Aguirre-Soto − *School of Engineering and Sciences, Tecnologico de Monterrey, Monterrey, N.L. 64849, Mexico;* orcid.org/0000-0003-0455-5401

Complete contact information is available at: https://pubs.acs.org/10.1021/jacs.1c04236

Author Contributions

The paper was written through contributions of all authors.

Notes

The authors declare no competing financial interest.

ACKNOWLEDGMENTS

This work was supported by the National Research Foundation of Singapore through the Antimicrobial Resistance Interdisciplinary Research Group and the MISTI MIT-Mexico Seed Fund. S.K. acknowledges support from the Kwanjeong Educational Foundation. A.A.-S. acknowledges a CONACYT Postdoctoral Research Award (263622). The authors thank Yining Hao and Dousabel M. Y. Tay for sharing affinity proteins (biotinylated MBP-SsoNP.E1, SsoNP.E2-CBD, and rcSso7d.SA-CBD) and SARS-CoV-2 nucleocapsid protein that they expressed and purified.

REFERENCES

(1) Kozel, T. R.; Burnham-Marusich, A. R. Point-of-Care Testing for Infectious Diseases: Past, Present, and Future. *J. Clin. Microbiol.* **2017**, *55*, 2313−2320.

(2) Chen, H.; Liu, K.; Li, Z.; Wang, P. Point-of-Care Testing for Infectious Diseases. *Clin. Chim. Acta* **2019**, *493*, 138−147.

(3) Uyeki, T. M.; Prasad, R.; Vukotich, C.; Stebbins, S.; Rinaldo, C. R.; Ferng, Y.-H.; Morse, S. S.; Larson, E. L.; Aiello, A. E.; Davis, B.; Monto, A. S. Low Sensitivity of Rapid Diagnostic Test for Influenza. *Clin. Infect. Dis.* **2009**, *48*, No. e89.

(4) Vasoo, S.; Stevens, J.; Singh, K. Rapid Antigen Tests for Diagnosis of Pandemic (Swine) Influenza A/H1N1. *Clin. Infect. Dis.* **2009**, *49*, 1090−1093.

(5) Perchetti, G. A.; Huang, M.-L.; Mills, M. G.; Jerome, K. R.; Greninger, A. L. Analytical Sensitivity of the Abbott BinaxNOW COVID-19 Ag CARD. *J. Clin. Microbiol.* **2021**, *59*, No. e02880.

(6) Erlich, H. A.; Gelfand, D.; Sninsky, J. J. Recent Advances in the Polymerase Chain Reaction. *Science* **1991**, *252*, 1643−1651.

(7) Sano, T.; Smith, C. L.; Cantor, C. R. Immuno-PCR: Very Sensitive Antigen Detection by Means of Specific Antibody-DNA Conjugates. *Science* **1992**, *258*, 120−122.

(8) Niemz, A.; Ferguson, T. M.; Boyle, D. S. Point-of-Care Nucleic Acid Testing for Infectious Diseases. *Trends Biotechnol.* **2011**, *29* (5), 240−250.

(9) Zhao, Y.; Chen, F.; Li, Q.; Wang, L.; Fan, C. Isothermal Amplification of Nucleic Acids. *Chem. Rev.* **2015**, *115*, 12491−12545.

(10) Kilic, T.; Weissleder, R.; Lee, H. Molecular and Immunological Diagnostic Tests of COVID-19: Current Status and Challenges. *iScience* **2020**, *23* (8), 101406.

(11) Craw, P.; Balachandran, W. Isothermal Nucleic Acid Amplification Technologies for Point-of-Care Diagnostics: A Critical Review. *Lab Chip* **2012**, *12* (14), 2469.
(12) Kumar, S.; Gallagher, R.; Bishop, J.; Kline, E.; Buser, J.; Lafleur, L.; Shah, K.; Lutz, B.; Yager, P. Long-Term Dry Storage of Enzyme-Based Reagents for Isothermal Nucleic Acid Amplification in a Porous Matrix for Use in Point-of-Care Diagnostic Devices. *Analyst* **2020**, *145*, 6875−6886.
(13) Zhang, Y.; Ozdemir, P. Microfluidic DNA Amplification-A Review. *Anal. Chim. Acta* **2009**, *638*, 115−125.
(14) Yoon, H. J.; Mirkin, C. A. PCR-like Cascade Reactions in the Context of an Allosteric Enzyme Mimic. *J. Am. Chem. Soc.* **2008**, *130* (35), 11590−11591.
(15) Sella, E.; Shabat, D. Dendritic Chain Reaction. *J. Am. Chem. Soc.* **2009**, *131*, 9934−9936.
(16) Yoshii, T.; Onogi, S.; Shigemitsu, H.; Hamachi, I. Chemically Reactive Supramolecular Hydrogel Coupled with a Signal Amplification System for Enhanced Analyte Sensitivity. *J. Am. Chem. Soc.* **2015**, *137* (9), 3360−3365.
(17) Pallu, J.; Rabin, C.; Creste, G.; Branca, M.; Mavré, F.; Limoges, B. Exponential Molecular Amplification by H_2O_2-Mediated Autocatalytic Deprotection of Boronic Ester Probes to Redox Cyclers. *Chem. - Eur. J.* **2019**, *25* (31), 7534−7546.
(18) Perry-Feigenbaum, R.; Sella, E.; Shabat, D. Autoinductive Exponential Signal Amplification: A Diagnostic Probe for Direct Detection of Fluoride. *Chem. - Eur. J.* **2011**, *17*, 12123−12128.
(19) Baker, M. S.; Phillips, S. T. A Two-Component Small Molecule System for Activity-Based Detection and Signal Amplification: Application to the Visual Detection of Threshold Levels of Pd(II). *J. Am. Chem. Soc.* **2011**, *133*, 5170−5173.
(20) Baker, M. S.; Phillips, S. T. A Small Molecule Sensor for Fluoride Based on an Autoinductive, Colorimetric Signal Amplification Reaction. *Org. Biomol. Chem.* **2012**, *10*, 3595−3599.
(21) Gu, J. A.; Mani, V.; Huang, S.-T. Design and Synthesis of Ultrasensitive Off-On Fluoride Detecting Fluorescence Probe via Autoinductive Signal Amplification. *Analyst* **2015**, *140*, 346−352.
(22) Sun, X.; Dahlhauser, S. D.; Anslyn, E. V. New Autoinductive Cascade for the Optical Sensing of Fluoride: Application in the Detection of Phosphoryl Fluoride Nerve Agents. *J. Am. Chem. Soc.* **2017**, *139*, 4635−4638.
(23) Sun, X.; Anslyn, E. V. An Auto-Inductive Cascade for the Optical Sensing of Thiols in Aqueous Media: Application in the Detection of a VX Nerve Agent Mimic. *Angew. Chem., Int. Ed.* **2017**, *56*, 9522−9526.
(24) Mohapatra, H.; Schmid, K. M.; Phillips, S. T. Design of Small Molecule Reagents That Enable Signal Amplification via an Autocatalytic, Base-Mediated Cascade Elimination Reaction. *Chem. Commun.* **2012**, *48*, 3018−3020.
(25) Kottani, R.; Majjigapu, J. R. R.; Kurchan, A.; Majjigapu, K.; Gustafson, T. P.; Kutateladze, A. G. Photoinduced Signal Amplification through Controlled Externally Sensitized Fragmentation in Masked Sensitizers. *J. Am. Chem. Soc.* **2006**, *128* (46), 14794−14795.
(26) Gustafson, T. P.; Metzel, G. A.; Kutateladze, A. G. Photochemically Amplified Detection of Molecular Recognition Events: An Ultra-Sensitive Fluorescence Turn-Off Binding Assay. *Org. Biomol. Chem.* **2011**, *9*, 4752−4755.
(27) Blackmond, D. G. An Examination of the Role of Autocatalytic Cycles in the Chemistry of Proposed Primordial Reactions. *Angew. Chem., Int. Ed.* **2009**, *48*, 386−390.
(28) Goggins, S.; Frost, C. G. Approaches Towards Molecular Amplification for Sensing. *Analyst* **2016**, *141* (11), 3157−3218.
(29) Uchida, K.; Koizumi, M. Photosensitized Oxidation of Leuco-Uranine. II. Kinetics of an Acridine-Sensitized Photoöxidation in the Deaerated Solution. *Bull. Chem. Soc. Jpn.* **1962**, *35* (11), 1875−1881.
(30) Usui, Y.; Iwanaga, C.; Koizumi, M. Reactions of Singlet Oxygen and Half-Reduced Oxygen Which Are Produced Simultaneously by the Interaction of Triplet Dye and Oxygen. *Bull. Chem. Soc. Jpn.* **1969**, *42*, 1231−1239.
(31) Krüger, U.; Memming, R. Formation and Reactions of Long Lived Xanthene Dye Radicals. I. Photochemical Studies on Reactions of Semireduced Fluoresceïn. *Berichte der Bunsen-Gesellschaft für Phys. Chemie* **1974**, *78* (7), 670−678.
(32) Wardman, P. Fluorescent and Luminescent Probes for Measurement of Oxidative and Nitrosative Species in Cells and Tissues: Progress, Pitfalls, and Prospects. *Free Radical Biol. Med.* **2007**, *43* (7), 995−1022.
(33) Wrona, M.; Patel, K. B.; Wardman, P. The Roles of Thiol-Derived Radicals in the Use of 2′,7′-Dichlorodihydrofluorescein as a Probe for Oxidative Stress. *Free Radical Biol. Med.* **2008**, *44*, 56−62.
(34) Daghastanli, N. A.; Itri, R.; Baptista, M. S. Singlet Oxygen Reacts with 2′,7′-Dichlorodihydrofluorescein and Contributes to the Formation of 2′,7′-Dichlorofluorescein. *Photochem. Photobiol.* **2008**, *84*, 1238−1243.
(35) Deerinck, T. J.; Martone, M. E.; Lev-Ram, V.; Green, D. P. L.; Tsien, R. Y.; Spector, D. L.; Huang, S.; Ellisman, M. H. Fluorescence Photooxidation with Eosin: A Method for High Resolution Immunolocalization and In Situ Hybridization Detection for Light and Electron Microscopy. *J. Cell Biol.* **1994**, *126* (4), 901−910.
(36) Hansen, R. R.; Sikes, H. D.; Bowman, C. N. Visual Detection of Labeled Oligonucleotides Using Visible-Light-Polymerization-Based Amplification. *Biomacromolecules* **2008**, *9*, 355−362.
(37) Johnson, G. A.; Muthukrishnan, N.; Pellois, J. P. Photoinactivation of Gram Positive and Gram Negative Bacteria with the Antimicrobial Peptide $(KLAKLAK)_2$ Conjugated to the Hydrophilic Photosensitizer Eosin Y. *Bioconjugate Chem.* **2013**, *24*, 114−123.
(38) Bowers, P. G.; Porter, G. Triplet State Quantum Yields for Some Aromatic Hydrocarbons and Xanthene Dyes in Dilute Solution. *Proc. R. Soc. London A. Math. Phys. Sci.* **1967**, *299*, 348−353.
(39) Encinas, M. V.; Rufs, A. M.; Bertolotti, S. G.; Previtali, C. M. Xanthene Dyes/Amine as Photoinitiators of Radical Polymerization: A Comparative and Photochemical Study in Aqueous Medium. *Polymer* **2009**, *50* (13), 2762−2767.
(40) Bilski, P.; Dabestani, R.; Chignell, C. F. Photoprocesses of Eosine and Rose Bengal Ion Pairs with Cationic Surfactant in Non-Polar Solvent: Application in Photosensitization Studies. *J. Photochem. Photobiol., A* **1994**, *79*, 121−130.
(41) Zhang, J.; Sun, L.; Yoshida, T. Spectroelectrochemical Studies on Redox Reactions of Eosin Y and Its Polymerization with Zn^{2+} Ions. *J. Electroanal. Chem.* **2011**, *662*, 384−395.
(42) Weng, G.; Mahmoud, M. A.; El-Sayed, M. A. Nanocatalysts Can Change the Number of Electrons Involved in Oxidation-Reduction Reaction with the Nanocages Being the Most Efficient. *J. Phys. Chem. C* **2012**, *116*, 24171−24176.
(43) Aguirre-Soto, A.; Kaastrup, K.; Kim, S.; Ugo-Beke, K.; Sikes, H. D. Excitation of Metastable Intermediates in Organic Photoredox Catalysis: Z-Scheme Approach Decreases Catalyst Inactivation. *ACS Catal.* **2018**, *8*, 6394−6400.
(44) Uchida, K.; Koizumi, M. Photosensitized Oxidation of Leuco-Uranine. I. Qualitative Studies of the Nature of the Reaction in the Deaerated Solution. *Bull. Chem. Soc. Jpn.* **1962**, *35* (11), 1871−1875.
(45) Uchida, K. The Photosensitized Oxidation of Leuco-Uranine. III. The Kinetics of an Acridine-Sensitized Photoöxidation in an Aerated Solution. *Bull. Chem. Soc. Jpn.* **1963**, *36* (9), 1097−1106.
(46) Görner, H. Oxygen Uptake Induced by Electron Transfer from Donors to the Triplet State of Methylene Blue and Xanthene Dyes in Air-Saturated Aqueous Solution. *Photochem. Photobiol. Sci.* **2008**, *7*, 371−376.
(47) Krüger, U.; Memming, R. Formation and Reactions of Long Lived Xanthene Dye Radicals. II. Photochemical Reduction of Rhodamine-B and Fluoresceïn Derivatives. *Berichte der Bunsen-Gesellschaft für Phys. Chemie* **1974**, *78* (7), 679−685.
(48) Concentration of dissolved oxygen in water. http://water.usgs.gov/software/DOTABLES (Accessed on April 2021).
(49) Kralik, P.; Kusic, H.; Koprivanac, N.; Bozic, A. L. Degradation of Chlorinated Hydrocarbons by UV/H_2O_2: The Application of Experimental Design and Kinetic Modeling Approach. *Chem. Eng. J.* **2010**, *158* (2), 154−166.

https://doi.org/10.1021/jacs.1c04236
J. Am. Chem. Soc. 2021, 143, 11544−11553

(50) Rizzuto, F.; Spikes, J. D. The Eosin-Sensitized Photooxidation of Substituted Phenylalanines and Tyrosines. *Photochem. Photobiol.* **1977**, *25*, 465−476.
(51) Wilkinson, F.; Brummer, J. G. Rate Constants for the Decay and Reactions of the Lowest Electronically Excited Singlet State of Molecular Oxygen in Solution. *J. Phys. Chem. Ref. Data* **1981**, *10* (4), 809−999.
(52) DeRosa, M. C.; Crutchley, R. J. Photosensitized Singlet Oxygen and Its Applications. *Coord. Chem. Rev.* **2002**, *233*−*234*, 351−371.
(53) Trashin, S.; Rahemi, V.; Ramji, K.; Neven, L.; Gorun, S. M.; De Wael, K. Singlet Oxygen-Based Electrosensing by Molecular Photosensitizers. *Nat. Commun.* **2017**, *8*, 16108.
(54) Foote, C. S. Photosensitized Oxygenations and the Role of Singlet Oxygen. *Acc. Chem. Res.* **1968**, *1* (4), 104−110.
(55) Schmidt, R.; Drews, W.; Brauer, H.-D. Wavelength-Dependent Photostable or Photoreversible Photochromic System. *J. Phys. Chem.* **1982**, *86*, 4909−4913.
(56) Maeda, H.; Nanai, Y.; Mizuno, K.; Chiba, J.; Takeshima, S.; Inouye, M. Photooxygenation of Alkynylperylenes. Formation of Dibenzo[*jk*,*mn*]phenanthrene-4,5-diones. *J. Org. Chem.* **2007**, *72*, 8990−8993.
(57) Filatov, M. A.; Baluschev, S.; Landfester, K. Protection of Densely Populated Excited Triplet State Ensembles against Deactivation by Molecular Oxygen. *Chem. Soc. Rev.* **2016**, *45* (17), 4668−4689.
(58) Tratnyek, P. G.; Holgné, J. Oxidation of Substituted Phenols in the Environment: A QSAR Analysis of Rate Constants for Reaction with Singlet Oxygen. *Environ. Sci. Technol.* **1991**, *25*, 1596−1604.
(59) Al-Nu'Airat, J.; Dlugogorski, B. Z.; Gao, X.; Zeinali, N.; Skut, J.; Westmoreland, P. R.; Oluwoye, I.; Altarawneh, M. Reaction of Phenol with Singlet Oxygen. *Phys. Chem. Chem. Phys.* **2019**, *21*, 171−183.
(60) Bonneau, R.; Pottier, R.; Joussot-Dubien, J. pH Dependence of Singlet Oxygen Production in Aqueous Solutions Using Thiazine Dyes as Photosensitizers. *Photochem. Photobiol.* **1975**, *21*, 159−163.
(61) Ehrenberg, B.; Anderson, J. L.; Foote, C. S. Kinetics and Yield of Singlet Oxygen Photosensitized by Hypericin in Organic and Biological Media. *Photochem. Photobiol.* **1998**, *68* (2), 135−140.
(62) Majek, M.; Filace, F.; Jacobi von Wangelin, A. On the Mechanism of Photocatalytic Reactions with Eosin Y. *Beilstein J. Org. Chem.* **2014**, *10*, 981−989.
(63) Aguirre-Soto, A.; Kim, S.; Kaastrup, K.; Sikes, H. D. On the Role of N-Vinylpyrrolidone in the Aqueous Radical-Initiated Copolymerization with PEGDA Mediated by Eosin Y in the Presence of O_2. *Polym. Chem.* **2019**, *10* (8), 926−937.
(64) Jarnikova, E. S.; Parkhats, M. V.; Stasheuski, A. S.; Lepeshkevich, S. V.; Dzhagarov, B. M. Quantum Yield and Rate Constant of the Singlet $^1\Delta_g$ Oxygen Luminescence in an Aqueous Medium in the Presence of Nanoscale Inhomogeneities. *Opt. Spectrosc.* **2017**, *122* (4), 596−601.
(65) Penzkofer, A.; Tyagi, A.; Slyusareva, E.; Sizykh, A. Phosphorescence and Delayed Fluorescence Properties of Fluorone Dyes in Bio-Related Films. *Chem. Phys.* **2010**, *378*, 58−65.
(66) Natera, J. E.; Massad, W. A.; Amat-Guerri, F.; García, N. A. Elementary Processes in the Eosin-Sensitized Photooxidation of 3,3′-Diaminobenzidine for Correlative Fluorescence and Electron Microscopy. *J. Photochem. Photobiol., A* **2011**, *220* (1), 25−30.
(67) Seligman, A. M.; Karnovsky, M. J.; Wasserkrug, H. L.; Hanker, J. S. Nondroplet Ultrastructural Demonstration of Cytochrome Oxidase Activity with a Polymerizing Osmiophilic Reagent, Diaminobenzidine (DAB). *J. Cell Biol.* **1968**, *38*, 1−14.
(68) Bar-On, Y. M.; Flamholz, A.; Phillips, R.; Milo, R. SARS-CoV-2 (COVID-19) by the Numbers. *eLife* **2020**, *9*, 1−15.
(69) Carter, L. J.; Garner, L. V.; Smoot, J. W.; Li, Y.; Zhou, Q.; Saveson, C. J.; Sasso, J. M.; Gregg, A. C.; Soares, D. J.; Beskid, T. R.; Jervey, S. R.; Liu, C. Assay Techniques and Test Development for COVID-19 Diagnosis. *ACS Cent. Sci.* **2020**, *6* (5), 591−605.
(70) Weissleder, R.; Lee, H.; Ko, J.; Pittet, M. J. COVID-19 Diagnostics in Context. *Sci. Transl. Med.* **2020**, *12*, No. eabc1931.
(71) Kim, S.; Yee, E.; Miller, E. A.; Hao, Y.; Tay, D. M. Y.; Sung, K.-J.; Jia, H.; Johnson, J. M.; Ball, A.; Conway, H.; Saeed, M.; Mace, C. R.; Yurt, D. Y.; Sikes, H. D. Developing a SARS-CoV-2 Antigen Test Using Engineered Affinity Proteins. 2021.04.19, *ChemRxiv*. https://chemrxiv.org/engage/chemrxiv/article-details/60c757a6469df4a17df454fb. (accessed **2021**-06−25).
(72) Pollock, N. R.; Savage, T. J.; Wardell, H.; Lee, R. A.; Mathew, A.; Stengelin, M.; Sigal, G. B. Correlation of SARS-CoV-2 Nucleocapsid Antigen and RNA Concentrations in Nasopharyngeal Samples from Children and Adults Using an Ultrasensitive and Quantitative Antigen Assay. *J. Clin. Microbiol.* **2021**, *59* (4), No. e03077.
(73) Gniazdowski, V.; Morris, C. P.; Wohl, S.; Mehoke, T.; Srividya, R.; Thielen, P.; Powell, H.; Smith, B.; Armstrong, D. T.; Herrera, M.; Reifsnyder, C.; Sevdali, M.; Carroll, K. C.; Pekosz, A.; Mostafa, H. H. Repeat COVID-19 Molecular Testing: Correlation with Recovery of Infectious Virus, Molecular Assay Cycle Thresholds, and Analytical Sensitivity. 2020.08.06, *Clin. Infect. Dis.* https://www.medrxiv.org/content/10.1101/2020.08.05.20168963v1. (accessed **2020**-06−25). DOI: 10.1093/cid/ciaa1616
(74) La Scola, B.; Le Bideau, M.; Andreani, J.; Hoang, V. T.; Grimaldier, C.; Colson, P.; Gautret, P.; Raoult, D. Viral RNA Load as Determined by Cell Culture as a Management Tool for Discharge of SARS-CoV-2 Patients from Infectious Disease Wards. *Eur. J. Clin. Microbiol. Infect. Dis.* **2020**, *39* (6), 1059−1061.
(75) Jaafar, R.; Aherfi, S.; Wurtz, N.; Clio, G.; Hoang, V. T.; Colson, P.; Raoult, D.; La Scola, B. Corrleation Between 3790 Quantitative Polymerase Chain Reaction-Positives Samples and Positive Cell Cultures, Including 1941 Severe Acute Respiratory Syndrome Coronavirus 2 Isolates. *Clin. Infect. Dis.* **2021**, *72*, No. ciaa1491.
(76) Broughton, J. P.; Deng, X.; Yu, G.; Fasching, C. L.; Servellita, V.; Singh, J.; Miao, X.; Streithorst, J. A.; Granados, A.; Sotomayor-Gonzalez, A.; Zorn, K.; Gopez, A.; Hsu, E.; Gu, W.; Miller, S.; Pan, C.-Y.; Guevara, H.; Wadfod, D. A.; Chen, J. S.; Chiu, C. Y. CRISPR-Cas12-Based Detection of SARS-CoV-2. *Nat. Biotechnol.* **2020**, *38* (7), 870−874.
(77) Dao Thi, V. L.; Herbst, K.; Boerner, K.; Meurer, M.; Kremer, L. P. M.; Kirrmaier, D.; Freistaedter, A.; Papagiannidis, D.; Galmozzi, C.; Stanifer, M. L.; Boulant, S.; Klein, S.; Chlanda, P.; Khalid, D.; Miranda, I. B.; Schnitzler, P.; Kräusslich, H.-G.; Knop, M.; Anders, S. A Colorimetric RT-LAMP Assay and LAMP-Sequencing for Detecting SARS-CoV-2 RNA in Clinical Samples. *Sci. Transl. Med.* **2020**, *12*, No. eabc7075.
(78) Alafeef, M.; Dighe, K.; Moitra, P.; Pan, D. Rapid, Ultrasensitive, and Quantitative Detection of SARS-CoV-2 Using Antisense Oligonucleotides Directed Electrochemical Biosensor Chip. *ACS Nano* **2020**, *14* (12), 17028−17045.
(79) Mina, M. J.; Andersen, K. G. COVID-19 Testing: One Size Does Not Fit All. *Science* **2021**, *371* (6525), 126−128.
(80) Cevik, M.; Tate, M.; Lloyd, O.; Maraolo, A. E.; Schafers, J.; Ho, A. SARS-CoV-2, SARS-CoV, and MERS-CoV Viral Load Dynamics, Duration of Viral Shedding, and Infectiousness: A Systematic Review and Meta-Analysis. *Lancet Microbe* **2021**, *2* (1), E13−E22.
(81) Albert, E.; Torres, I.; Bueno, F.; Huntley, D.; Molla, E.; Fernández-Fuentes, M. A.; Martínez, M.; Poujois, S.; Forque, L.; Valdivia, A.; de la Asunción, C. S.; Ferrer, J.; Colomina, J.; Navarro, D. Field Evaluation of a Rapid Antigen Test (Panbio COVID-19 Ag Rapid Test Device) for COVID-19 Diagnosis in Primary Healthcare Centres. *Clin. Microbiol. Infect.* **2021**, *27* (3), 4 DOI: 10.1016/j.cmi.2020.11.004.
(82) Pekosz, A.; Cooper, C. K.; Parvu, V.; Li, M.; Andrews, J. C.; Manabe, Y. C.; Kodsi, S.; Leitch, J.; Gary, D. S.; Roger-Dalbert, C. Antigen-Based Testing But Not Real-Time PCR Correlates with SARS-CoV-2 Virus Culture. *Clin. Infect. Dis.* **2021**, No. ciaa1706.
(83) Miller, E. A.; Baniya, S.; Osorio, D.; Maalouf, Y. J. Al; Sikes, H. D. Paper-Based Diagnostics in the Antigen-Depletion Regime: High-Density Immobilization of rcSso7d-Cellulose-Binding Domain Fusion Proteins for Efficient Target Capture. *Biosens. Bioelectron.* **2018**, *102*, 456−463.

(84) Lathwal, S.; Sikes, H. D. Assessment of Colorimetric Amplification Methods in a Paper-Based Immunoassay for Diagnosis of Malaria. *Lab Chip* **2016**, *16* (8), 1374−1382.
(85) Uchida, K.; Kato, S.; Koizumi, M. Photosensitized Oxidation of Leuco-Uranine and the Identification of the Photobleached Product of Uranine in Ethanol Solution. *Bull. Chem. Soc. Jpn.* **1962**, *35* (1), 16−22.

https://doi.org/10.1021/jacs.1c04236
J. Am. Chem. Soc. 2021, 143, 11544−11553